6G for Connected Sky
“6G-SKY”

Work Package 2

Multi-Technology Connectivity Links

Task 2.2 – ATG Antenna Development Specific for Flying Vehicles

Deliverable 2.2.4
A2G Antenna Concept: Measurement results of the antenna systems

6G-SKY Project
10. June 2025

Abstract

Antenna design has a key role in network performance, especially in air-to-ground (ATG) communication systems. Mobile communication systems have been traditionally built to serve terrestrial users only, and the conventional ground base station (BS) antenna design needs to be revisited.

This deliverable presents the lab test results of the novel demonstrator antennas concept tailored for the emerging 7 GHz **cmWave** frequency band. The development process was marked by the complex challenge of integrating diverse disciplines, including electromagnetic behavior, mechanical design possibilities and tolerances, and practical construction techniques for small antenna geometries. Key findings from this project include insights into outbid limitations of current PCB design rules, which need innovative approaches to push technological boundaries. Additionally, the project underscored the importance of expertise in soldering techniques specific to small geometries, highlighting their critical role in ensuring the structural interaction and optimal performance of the antenna unit. This work sets the basis for future advancements in cmWave ultra large antenna arrays.

Participants in WP 2:

- Deutsche Telekom (WPL, TL)
- Ericsson AB, EAB (TL)
- KTH
- Fraunhofer
- Airbus
- EAG (TL)

Contributors in Task 2.2

- EAG, Ericsson Antenna Technology Germany GmbH (TL)
- Airbus
- Deutsche Telekom

6G-SKY, Work Package 2: Multi-Technology Connectivity Links

Task 2.2: ATG antenna development specific for flying vehicles

In tasks 2.2.1 to 2.2.3, a simulation framework was established that enables the investigation of antennas for the A2G communication link. Therefore, the requirement for the ground station antenna and of the different flying UE antenna systems have been defined. In the next step, an antenna was developed and the simulation results were presented.

Sub **Task 2.2.4**: Finally, this resulted to a prototypical implementation of ground base station antenna systems that can be used for demonstration purposes. First lab measurement results of the demonstrator antennas are shown in this document.

D2.2.4 A2G Antenna Concept: Measurement Results
Editor: Jan Graevendieck, (EAG)
Reviewer: Ramon Delgado Pulgar (EAB), Bastian Bertholdt (ADS)
Contributors: Martin Jacob (EAG)

6G-SKY

Deliverable 2.2.4

Editor: Jan Graevendieck, EAG

Project coordinator: Dominic Schupke, Airbus

Technical Project Coordinator: Cicek Cavdar, KTH

CELTIC published project result

Disclaimer for confidential CELTIC-Plus project reports

This document contains material, which is copyright of certain PARTICIPANTS and may not be reproduced or copied without permission. The information contained in this document is the proprietary confidential information of certain PARTICIPANTS and may not be disclosed except in accordance with the regulations agreed in the Project Consortium Agreement (PCA).

The commercial use of any information in this document may require a licence from the proprietor of that information.

Neither the PARTICIPANTS nor CELTIC-NEXT warrant that the information contained in this document is capable of use, or that use of the information is free from risk and accept no liability for loss or damage suffered by any person using the information.

Document History

Version	Date	Author(s)/Reviewer	Comment
1.0	05.06.2025	Jan Graevendieck (EAG)	Internal draft
1.1	09.06.2025	Ramon Delgado Pulgar (EAB)	Reviewed version
1.2	10.06.2025	Martin Jacob (EAG) Bastian Bertholdt (ADS)	Reviewed version
1.3	10.06.2025	Jan Graevendieck (EAG)	Picture increased
1.4	06.11.2025	Jan Graevendieck	Confidential removed

Executive Summary

This document presents a novel antenna concept for air-to-ground (ATG) communications in the 7 GHz frequency range. This phased array antenna is intended for a ground base station (BS), but the antenna concept can also be adapted for the airborne platforms.
A key innovation for 7 GHz is the use of three-dimensional radiator elements in printed circuit board (PCB) embodiment, which enables a very broadband and high-performance solution. To enhance the decoupling between antenna arrays, the design incorporates galvanic isolation walls between array columns and an additional decoupling surface (ADS) is applied over the entire array.
The antenna's performance was evaluated using electromagnetic simulations, and the design was implemented in functional hardware components, considering physical and manufacturing constraints. Two functional prototype antennas were constructed for evaluation and testing. The measurement results demonstrated strong alignment with simulation predictions, indicating the concept's viability. These outcomes suggest that the antenna concept is not only technically sound but also suitable for industrial-scale production and deployment in real-world communication systems.

List of Authors

- Jan Graevendieck (Ericsson Antenna Technology Germany GmbH)
- Martin Jacob (Ericsson Antenna Technology Germany GmbH)

Table of Contents

List of Abbreviations

A	Antenna aperture
ADS	Array decoupling surface
AoSA	Array of sub-arrays
ASN	Airspace & non-terrestrial networks
ATG	Air to ground
BS	Base station
CAD	Computer aided design
CAE	Computer aided engineering
cmWave	centimetric wave
D	Antenna directivity
EM	Electromagnetic
EAN	European Aviation Network
EDA	Electronic Design Automation
HPBW	Half-power beamwidth
KPI	Key performance indicator
NTN	Non-terrestrial network
PCB	Printed circuit board
RF	Radio frequency
SA	Sub-array
TRX	Transceiver
UE	User equipment
VNA	Vector Network Analyzer
WP	Work package

1 Introduction

The 6G-SKY project focuses on investigating a solution to enable reliable and robust connectivity for both aerial and ground users through a flexible and adaptive network architecture that incorporates multiple technologies, including satellite communications and direct air-to-ground (ATG) links. Work Package 2 (WP2) primarily aims to identify and validate the optimal link parameters and antenna systems to address the unique challenges presented by combined aircraft and non-terrestrial networks (ASN) communication channels. This work will provide input to a network design for airborne users and contribute to the design of NTN for terrestrial users.

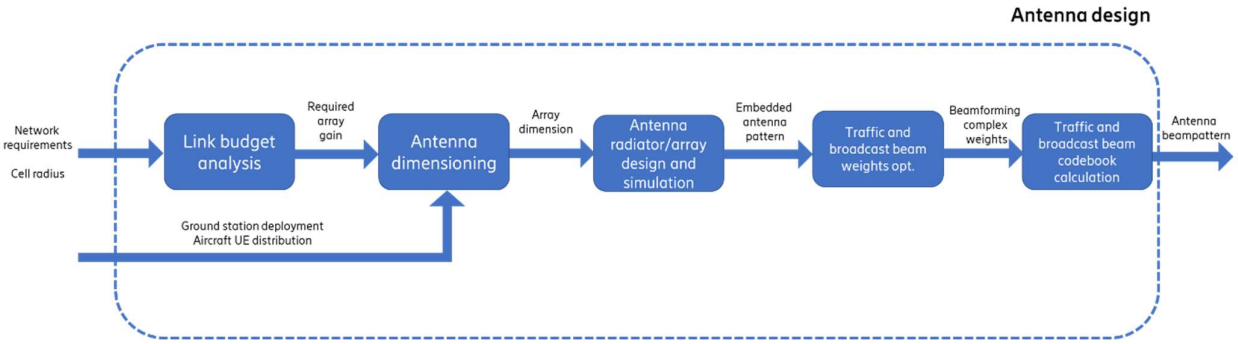

Figure 1.1 Antenna design flowchart.

A simulation framework was introduced in [1]. The framework consists of two main steps: antenna design and system-level performance evaluation. As shown in the flowchart of Figure 1.1, the antenna design itself consists of the following procedure:

1. Link budget analysis calculates necessary antenna gains for uplink and control channels to meet network targets.
2. Antenna dimensioning determines AoSA antenna dimensions based on required gains and network assumptions, including aircraft UE distribution.
3. The fully specified antenna is modeled in 3D using CAD tools and simulated with electromagnetic solvers to calculate embedded element patterns, accounting for mutual coupling effects.
4. Beamforming weights for traffic and broadcast antennas are calculated using these patterns to meet additional system requirements.
5. The complete antenna beam pattern is specified for both traffic and broadcast channels.

Once the results of the preliminary development steps were deemed satisfactory, the antenna concept and the corresponding requirements for the ground base station antenna were clearly defined. This enabled the initiation of the subsequent detailed development phases for the complete antenna array. A comprehensive overview of these development activities is documented in the 6G-Sky Memorandum 2.2 [2]. These efforts culminated in the prototypical implementation of ground base station antenna systems designed for direct air-to-ground communication links.

→ This document presents initial laboratory measurement results of the demonstrator antenna design. These results serve as a baseline for evaluating the feasibility of implementing the proposed antenna concept as a phased array system operating across the 6.4 GHz to 8.4 GHz frequency range.

1.1 Objective

The general objective of this document is to present the measurement result of two realized demonstrator antenna array.
The two realized setups differ in the interconnection network which connects the individual sub-sub-arrays per antenna column to a common antenna port on the back of the antenna. One network was realized for an antenna setup with zero degree tilt and one for a tilt of 10 degrees. This allowed us to measure two antennas, one with zero degrees and one with 10 degrees.

The specific objectives of this document are:

- To evaluate the designed building methodology.
- To confirm the EM simulation results and the antenna concept.
- To present the measurement results for the ground BS antenna performance in terms of scattering parameters and far-field beam pattern analysis.

1.2 Structure of the Document

Chapter 2 introduces the 7 GHz antenna concept for the ground BS antenna, and the assembly and realization of the measured prototype antennas is briefly described. The measured test results are presented in Chapter 3 scattering parameters and Chapter 4 beam pattern results. The concluding remarks are outlined in Chapter 5.

2 Antenna Concept for Ground Base Station

The ground BS antenna is designed to operate in the upcoming frequency spectrum of 6.4 GHz to 8.4 GHz, also called the cmWave band, and it features robust beamforming capabilities to effectively serve the airborne users. As we move towards these higher frequencies, the manufacturing of antenna elements at this frequency range presents its own set of challenges. The very small geometries required for these elements demand precise and innovative manufacturing solutions. As the industry advances, there is a growing need for new techniques that can produce these small-scale antenna elements efficiently and cost-effectively. These new manufacturing aspects are pivotal in shaping the future of communication systems at 7 GHz, influencing not only the design and production but also impacting overall system efficiency and reliability.
To support wide-area coverage, a key design consideration is the deployment of ultra-large antenna arrays that enable massive MIMO technologies. This is essential for enhancing the overall capacity of communication systems and ensuring seamless communication between ground-based nodes and flying objects such as aircraft and drones. Therefore, a scalable antenna concept was adopted here, allowing for flexible realization of various antenna apertures to meet different deployment requirements.

2.1 Design Overview

The entire antenna system consists of several functional units, which are:

1. The individual radiator element, which contains two antenna elements—one for +45° linear polarization and the other for -45° linear polarization. Baluns are integrated into the radiator bases and feed structure.
2. The antenna reflector, which also contains the feed and power divider network for three vertically aligned antenna elements. Additionally, isolation walls are integrated into the reflector board to separate the vertical antenna columns.
3. The backplane PCBs, where the combination network for the blocks of three antenna elements is implemented. This network also defines the antenna tilt.
4. The radome, which includes integrated ADS (Array Decoupling Structures).
5. The mechanical support structure for the antenna array, made of bent aluminum sheet metal.

The individual functional units are described in more detail in the next section of the document.

2.1.1 Radiating element

For the dual-polarized radiating elements, a cross-dipole patch antenna design was selected, making it an optimal choice for base station antenna. This configuration enables broadband frequency solution combined with high radiating efficiency The dual-polarized radiation mode was realized by using two linear-polarization Marchand baluns to feed the cross-dipole patches orthogonally, and a wide impedance bandwidth was achieved by optimizing the Marchand balun and the cross-dipole patches.

A Marchand balun is a type of transmission line transformer that converts an unbalanced (single-ended) signal to a balanced (differential) signal, or vice versa. These baluns for the ±45 degrees dual-polarization are intended in the 90 degree crossed arranged pair of feeding base PCB's via coupling through the microstrip feed structures.

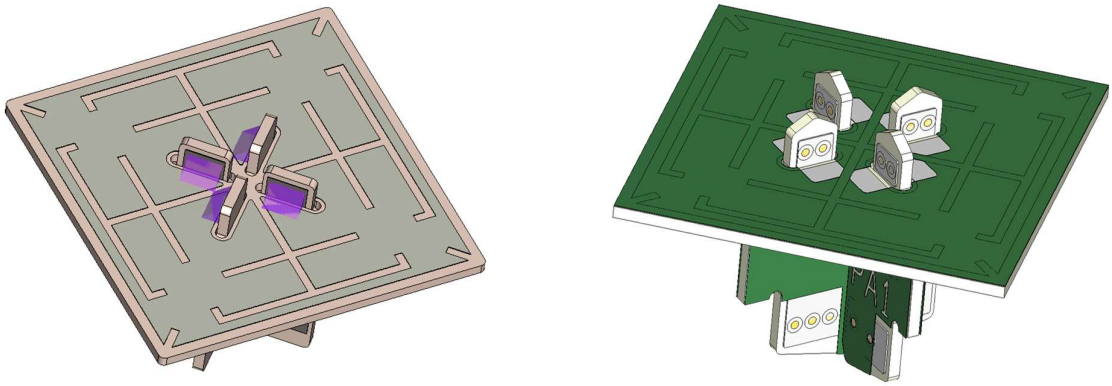

(a) EM CAE simulation model *(b) CAD model, PCB design*

Figure 2.1. Standalone dual polarized radiating element with a head size of 17 mm² and feed height of 6.5 mm.

This standalone antenna radiator is shown in Figure 2.1. Left picture (a) shows a representation from the 3d-EM simulation software with the PCB dielectric substrate and the conductive structures, the solder joints with solder are highlighted in purple here. In Figure 2.1 (b), the radiator model is assembled from the individual circuit boards as they come from the electronic layout system (EDA), taking into account the details of the PCB design rules and mechanical aspects.

2.1.2 Antenna Reflector and array configuration

The ground BS antenna consists of 144 Antenna elements (AE) configured in dual polarized (2x8) array of sub-arrays with (3x3) sub-array configurations as described in 6G-Sky Memorandum 2.2 [2]. Three radiator elements in elevation are electrically combined to form a 3-radiator block as sub-sub-array (3x1) configuration. Three of the sub-sub-blocks per antenna column are then interconnected via an additional combination board to one antenna port shown in Figure 2.5. With this configuration, the demonstrator antenna consists of 16 transceiver (TRX) ports and is designed for the frequency band 6400 MHz to 8400 MHz. This antenna configuration was realized, and the corresponding measurement results are presented in this document.

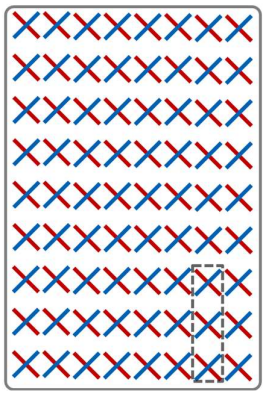

Figure 2.2. Antenna array with 8 columns and 9 dual polarized radiators per column.

A schematic front view of the antenna unit is shown in Figure 2.2. The antenna unit consists of 8 sub-arrays (two polarizations and 8 columns) and each sub-array has two coaxial-RF TRX ports for dual polarization. Each of the 72 displayed crosses symbolizes a radiating element. Each radiating element consists of two antenna elements oriented orthogonally to each other, with polarizations of +45°, shown in red, and –45°, shown in blue. A sub-sub-array consisting of three radiating elements is highlighted with dashed lines.

The antenna concept is designed to be modular, allowing for the realization of very large, so-called ultra-large antenna arrays. In the next illustration Figure 2.3, the antenna has been assembled with 768 antenna elements. The array configuration is dual-polarized (2x16) array of sub-arrays with (3x8) sub-array configurations. With this configuration, the antenna unit has 256 TRX ports.

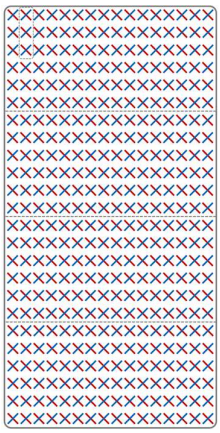

Figure 2.3. Antenna array 16 columns and 24 dual polarized radiators per column.

This modular concept has a column-to-column spacing of 21 mm which are $0.5\lambda_C$ at 7.2 GHz and the vertical spacing[1] is 29.35 mm which are $0.7\lambda_C$.at 7.2 GHz. This configuration allows to achieve directional beamforming in azimuth, where the columns can be used independently to serve different flying objects. This configuration allows to achieve a large directional beamforming in the azimuth direction. Whereas, in the elevation direction, the larger spacing allows beamforming only over a smaller area. However, this is sufficient because only a smaller angular range needs to be covered in

[1] Vertical spacing refers to row-to-row spacing, while horizontal spacing to column-to-column spacing.

the elevation direction. For more details, please refer to D2.2.3 ‘Ground Base Station Antenna Requirements’ [3].

The size difference, and consequently the antenna aperture, between these two antenna units is a factor of 5.3. This is reflected in the achievable antenna directivity.

- 144 AE unit, Figure 2.2, antenna size 264.15x168.0 mm²,
  Maximum antenna directivity[2] per antenna column[3] is 16.3 dBi for 7.4 GHz,
  Maximum antenna directivity[2] for the antenna unit[4] is 25.3 dBi for 7.4 GHz.

- 768 AE unit, Figure 2.3, antenna size 704.4x336.0 mm²,
  Maximum antenna directivity[2] per antenna column[3] is 20.5 dBi for 7.4 GHz,
  Maximum antenna directivity[2] for the antenna unit[4] is 32.6 dBi for 7.4 GHz.

2.1.3 Backplane interconnection board

Figure 2.4 shows the schematic of one antenna column with the 9 dual-polarized radiators and distribution network on sub-sub-array level. This network is placed on the base PCB of the hole antenna unit and functions also as the electrical reflector for the antenna elements. The diagram illustrates how three radiating elements are electrically combined at a single node via power dividers. For the sake of graphical clarity, only the network corresponding to the negative polarization is depicted.

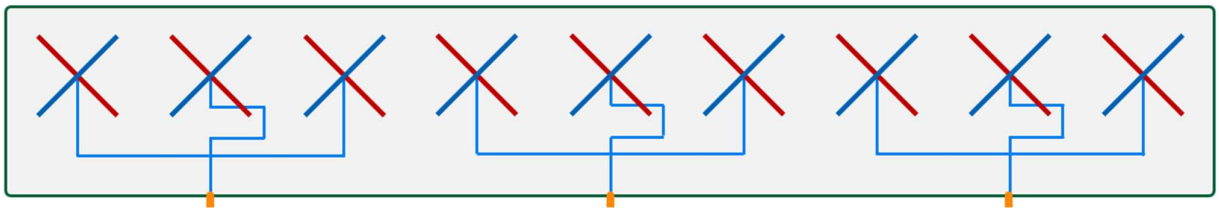

Figure 2.4. Schematic drawing of the interconnection of one polarization of one sub-sub-array. Three antenna elements are combined to one sub-sub-array

The three sub-sub-arrays described in Figure 2.4 were combined for the measurements into a single common feed point per antenna column and polarization. This was implemented using an additional board mounted on the rear side of the antenna, Figure 2.5 illustrates the complete signal path for a single antenna column and polarization. With this network, also the antenna tilt is tuned, therefore it is designed in such a way that the PCB could be easily replaced with other one with different relative signal lengths so that various antenna tilts are tunable. For our setup, two interchangeable printed circuit boards were used—one designed for 0° antenna tilt and the other for a 10° tilt. Instead of replacing these components, a continuously adjustable phase shifter could be implemented at this point.

[2] Calculation is based on the 3D-EM simulation results [2].

[3] This setup is representative of a typical broadcast beamforming scenario.

[4] This setup is representative of a typical traffic beamforming scenario.

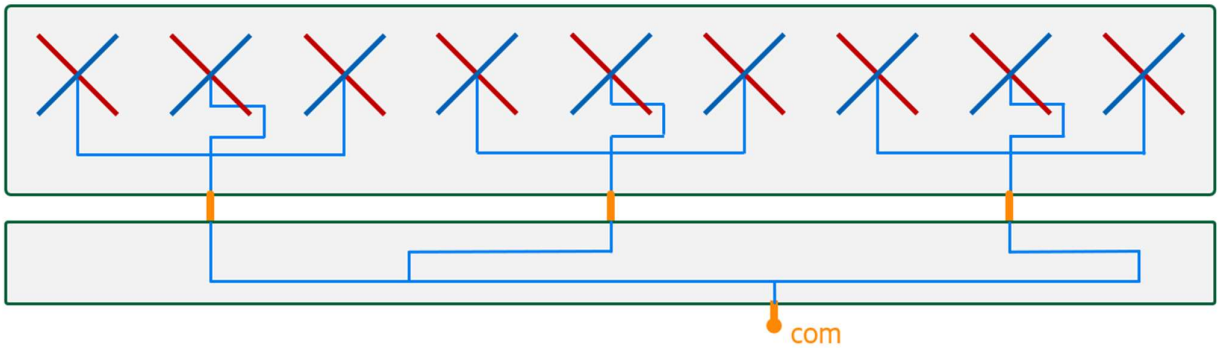

Figure 2.5. Schematic drawing of the interconnection of one polarization and one antenna column. The nine antenna elements are combined to one common RF port.

2.1.4 Array Decoupling Surface

The array decoupling surface (ADS) is a technology [4] that enhances the isolation between the radiating elements of an antenna array. The ground BS antenna uses the ADS to improve the isolation between the radiators and to reduce mutual coupling effects. Figure 2.6 shows the ADS in plain view.

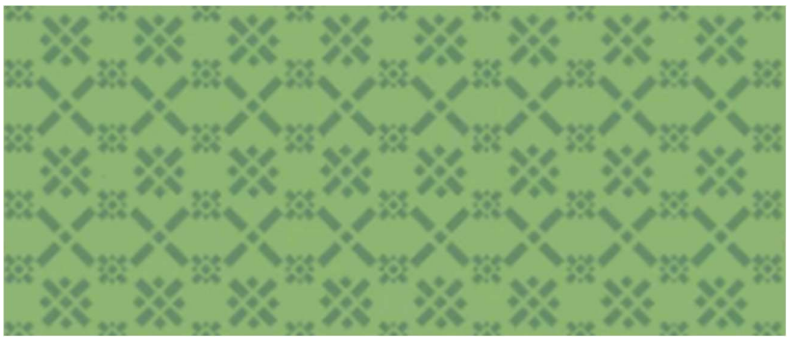

Figure 2.6. Segment of the ADS pattern.

The ADS works by creating an array of non-resonant passive elements that are placed above the radiators. An ADS is structured on a PCB with electrical small reflection patches. The electrical patches are designed to generate diffracted waves at the adjacent radiator to cancel the coupled waves, while minimizing the effect on the original array antenna. The reflected wave is super-positioned with the direct coupling path, resulting in some cancellation of the coupled wave at the neighboring radiator.
The ADS has a positive effect on the decoupling values between the columns. These values do not show a predefined tilt, so they are the worst-case values. With a fixed tilt, a further improvement in decoupling can be expected.

2.1.5 Mechanical assembly

Figure 2.7 shows the mechanical assembly of the 144 AE phased array antenna.
From top to bottom the antenna has following parts:

1. Radome with the integrated ADS pattern structure.
2. The radiating elements
3. Isolation walls for decoupling between antenna columns
4. Reflector board with integrated distribution network and connector to interconnect with the backplane network
5. Isolation foil to prevent galvanic contact from reflector board to the aluminum sheet metal caring structure
6. Aluminum sheet metal caring structure to mount the antenna
7. Backplane network that combines the sub-sub-arrays to one column antenna RF port

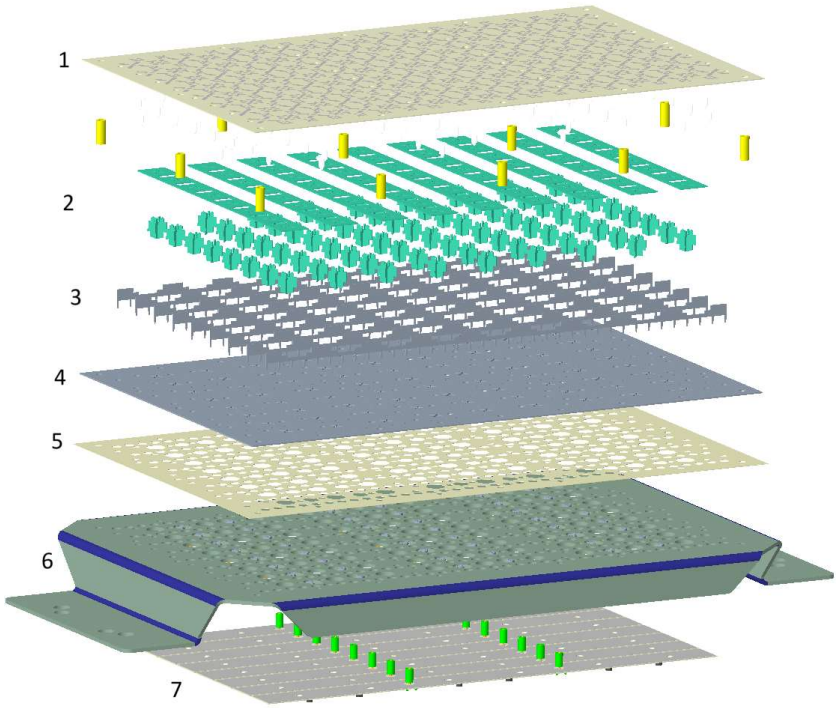

Figure 2.7. Exploded view of the mechanical assembly.

2.2 Realization of the antenna concept

Before the physical assembly of the antenna system could commence, several custom mechanical fixtures were developed and produced to ensure precise alignment and reliable connections. Among these were specially designed soldering jigs, which were used to accurately position and hold the components during the soldering process, like radiator bases and heads or the electrical isolation structures implemented between antenna columns. These fixtures were essential for maintaining

mechanical stability throughout the automated soldering process. The use of such tooling not only improved the repeatability of the process but also minimized the risk of misalignment, which could negatively impact the antenna's performance. The design of the jigs was tailored to the specific geometry of each element and took into account the thermal and mechanical constraints of the soldering procedure.
The following images Figure 2.8 and Figure 2.7 provide an insight into the assembly process of the antenna units.

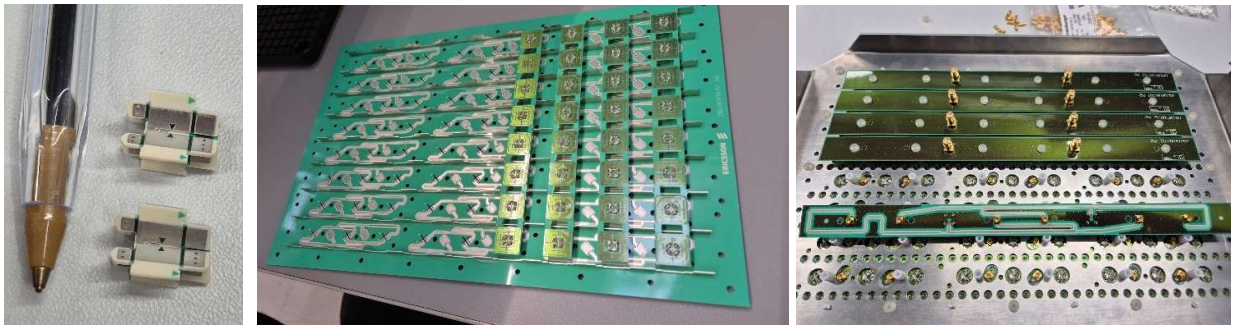

(a) Radiator feed *(b) Assembling of the antenna array* *(c) Assembling of the antenna backside*

Figure 2.8. Assembling and soldering of the antennas. Cross-mounted radiator feet (a), antenna reflector with the distribution network for the sub-arrays and the radiating elements (b), Antenna backside with the sub-array interconnection boards and the coaxial connectors (c).

Soldering capabilities is a pivotal and complex step in the assembly procedure of an antenna unit from small PCBs to preserving the array's performance. Automated soldering machines apply solder to the connection pads using techniques such as selective wave soldering. This ensures that all joints are electrically precise and mechanically accurate across all solder points.

(a) Size of the radiator head *(b) Radiator columns with separation walls*

Figure 2.9. Size comparison of a single radiator element with a euro coin (a), several radiating elements with the decoupling walls between the antenna columns (b).

3 Evaluation of the antenna scattering parameters

Scattering measurements involve directing electromagnetic waves at an object and capturing the reflected or transmitted signals using a vector network analyzer. Calibration of equipment is crucial to ensure accuracy in amplitude and phase measurements. The antennas must be in a controlled environment like an anechoic chamber, the chamber is lined with radio-frequency (RF) absorbing material that prevents reflections from walls, floor, and ceiling. This ensures that only the direct interaction between the antenna and the incident wave is measured without interference from unwanted multi-path signals. Figure 3.1. shows our used measurement setup.

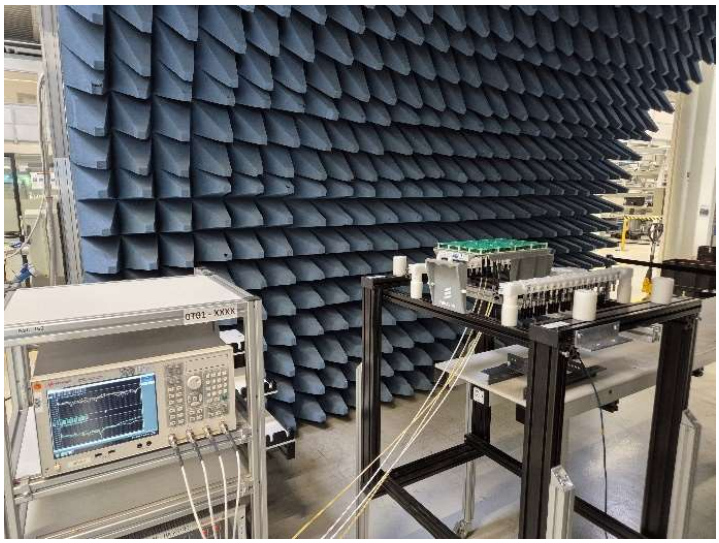

Figure 3.1.Picture of the measurement setup.

3.1 Scattering parameters of the antenna unit

Each of the 16 transceiver (TRX) antenna ports—corresponding to every antenna column and polarization combination—was measured using a vector network analyzer (VNA) to obtain both scalar and phase information. These measurements enabled the evaluation of all port return losses as well as the coupling between all port combinations.

In Figure 2, the port designations of the antenna unit are defined from the rear view. Due to the availability of only a 4-port vector network analyzer (VNA) for the frequency range under investigation, the measurements were conducted by frequently reconfiguring the connections between the VNA ports and the antenna ports. This procedure was carried out according to the switching mapping illustrated in Figure 3.

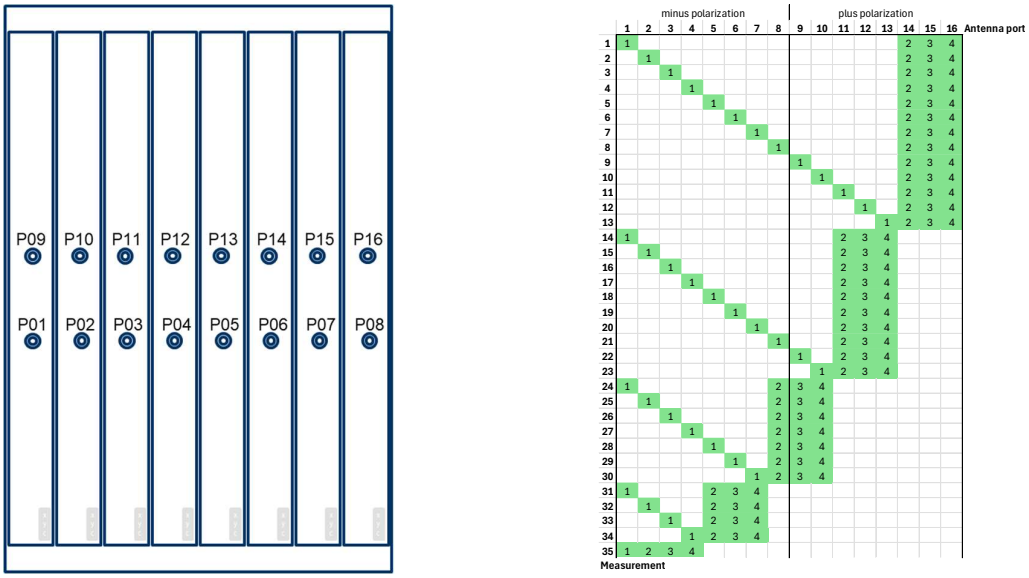

(a) Port mapping antenna *(b) Port mapping VNA*

Figure 3.2.Port mapping for the scattering parameter measurements with a 4-port VNA. (a) shows the mapping on the antenna backside and (b) the mapping to the VNA measurement device.

3.1.1 Antenna Unit with zero-degree tilt angle.

The antenna unit with the 0-degree tilt angle is measured, this unit is also labeled as antenna no. 1

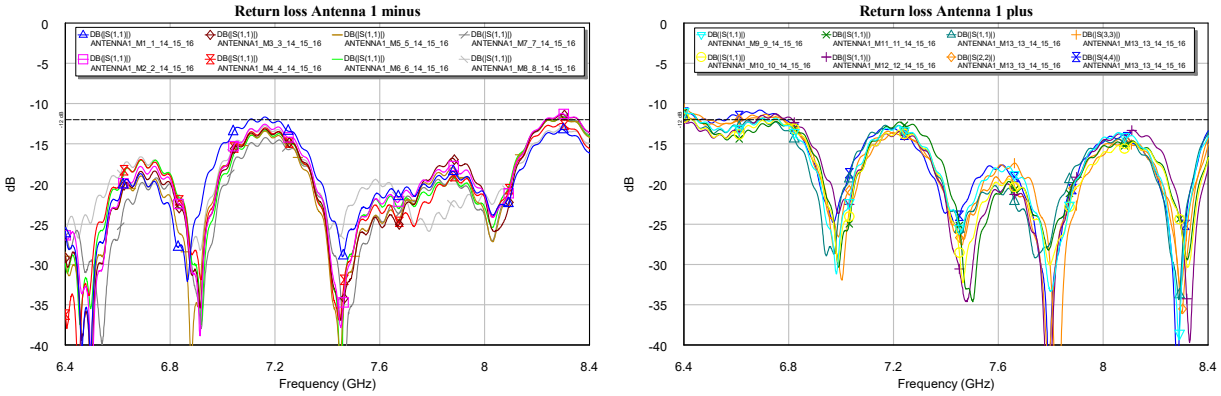

(a) Minus polarization ports *(b) Plus polarization ports*

Figure 3.3. Return losses for Antenna 1, all eight ports for the minus (a) and the plus (b) polarization.

Figure 3.3: All RF ports exhibit an impedance matching better than 12 dB within the envisaged frequency range. Within each polarization direction, the measurements show a highly consistent frequency response. The behavior of the plus and minus polarizations differs slightly, which is expected due to variations in signal routing and feed design between the two polarization paths.

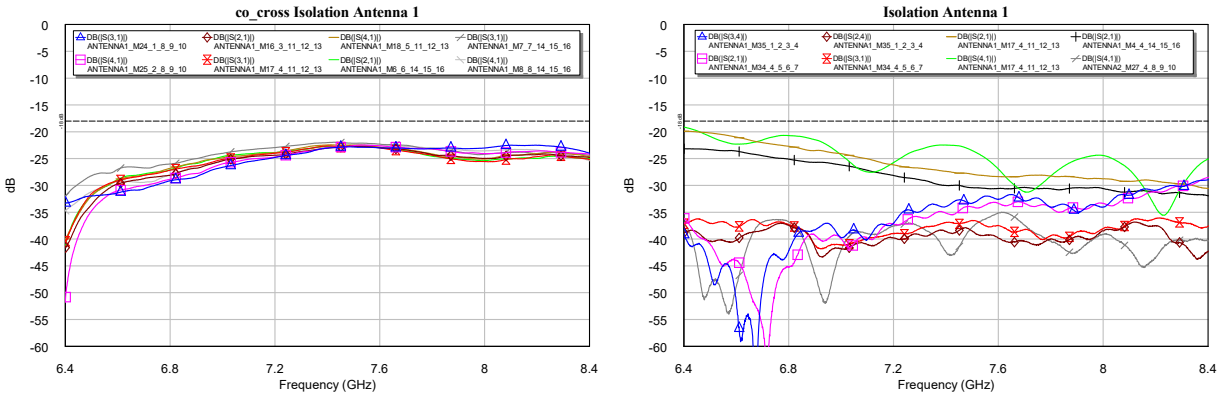

(a) Co-cross isolation *(b) Isolation between antenna columns*

Figure 3.4. Isolation antenna 1 between co- and cross-polarization within each antenna column (a) and to neighbor antenna columns (b).

Minimum isolation between the two antenna polarizations within the same sub-array or column shall be more than 20 dB. Figure 3.4 (a) demonstrates that these values were successfully achieved.
Figure 3.4 (b) shows the maximum coupling between any two antenna ports, in this figure, only the measurement curves with the highest coupling values are shown in order to maintain clarity.
The results indicate that the antenna equipped with the 0° tilt network exhibits favorable scattering parameter performance. Furthermore, the achieved impedance matching of 12 dB is considered a promising outcome for a first prototype, providing a solid foundation for further investigations.

3.1.2 Antenna unit with 10-degree tilt angle.

The antenna unit with the 10-degree tilt angle is measured, this unit is also labeled as antenna no. 2

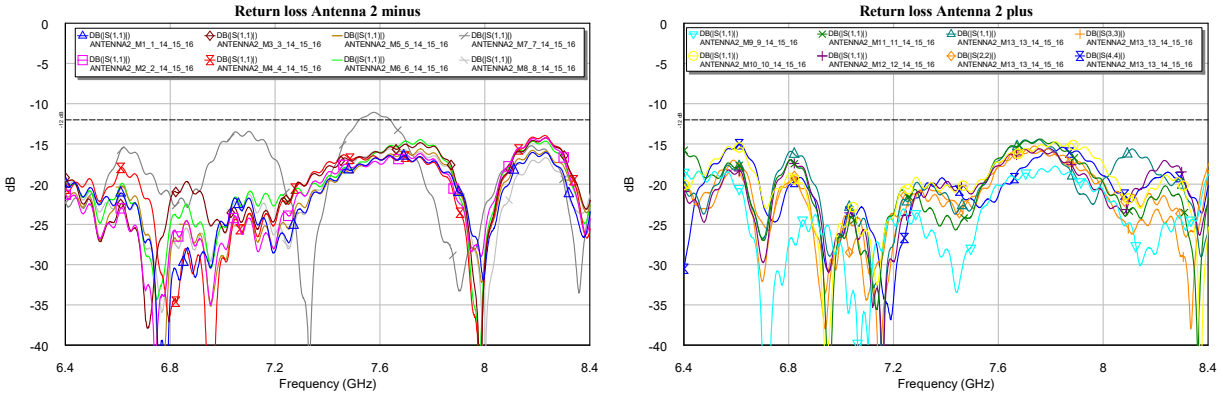

(a) Minus polarization ports *(b) Plus polarization ports*

Figure 3.5. Return losses for Antenna 2, all eight ports for the plus and the minus polarization.

Figure 3.5: All RF ports exhibit a good impedance matching better than the 0-degree tilted antenna. Within each polarization direction, the measurements show a highly consistent frequency response. An exception was observed at TRX port number 7, which exhibited anomalous behavior. This deviation is

both noticeable and unusual. Although initial investigations were conducted, no irregularities could be identified in the antenna hardware. Further analysis is necessary to understand the issue fully.
It is noticeable that, on average, the antenna matching is approximately 3 dB better than that of the antenna with 0° tilt. This improvement is expected, as the phase difference introduced by the feed network of the radiating elements partially compensates for the impedance mismatch of the individual antenna elements.

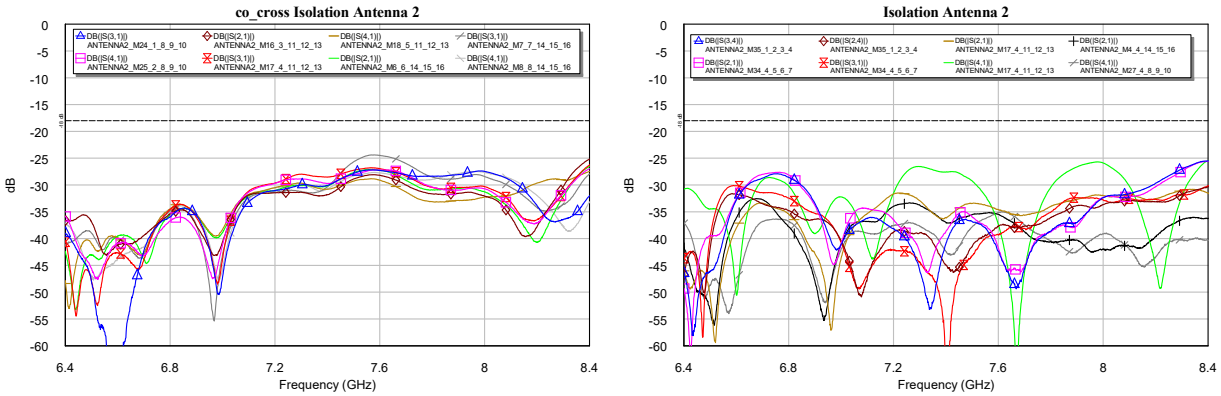

(a) Co-cross isolation *(b) Isolation between antenna columns*

Figure 3.6. Isolation antenna 2 between co- and cross-polarization within each antenna column and to neighbor antenna columns.

Minimum isolation between the two antenna polarizations within the same sub-array or column shall be more than 20 dB. Figure 3.6 (a) demonstrates that these values were successfully achieved.
Figure 3.6 (b) shows the maximum coupling between any two antenna ports, in this figure, only the measurement curves with the lowest coupling values are shown in order to maintain clarity.
Due to the 10° tilt network implemented in this antenna, the sub-sub-arrays are fed with a phase offset. As a result, the isolation between the two polarizations within a single antenna column exhibits more pronounced frequency-dependent variations. This effect can be observed by comparing Figure 3.4 (a) and Figure 3.6 (a).
In general, the 10° tilt antenna unit exhibits favorable scattering parameter performance. Furthermore, the achieved impedance matching of 15 dB is a very good result.

4 Evaluation of the antenna radiating pattern

The accurate measurement of far-field data is crucial for evaluating the performance of RF antennas. The far-field region refers to the area where the angular field distribution is independent of distance from the antenna, allowing for the characterization of antenna patterns, gain, and efficiency.
An anechoic chamber is specifically designed to simulate free-space conditions by absorbing reflections with its radio-frequency absorptive material. This controlled environment minimizes interference and ensures the accuracy of measurements. In our case, a compact antenna test range is used. Here, a plane wave is generated by a parabolic reflector assembly, also shown in Figure 4.3. The test antenna is positioned on a rotatable platform within the chamber. Precise alignment is critical to

ensure that the antenna's orientation corresponds accurately to its intended operational configuration. The platform facilitates the rotation of the antenna to measure radiation patterns in the azimuth and elevation planes at various angles.

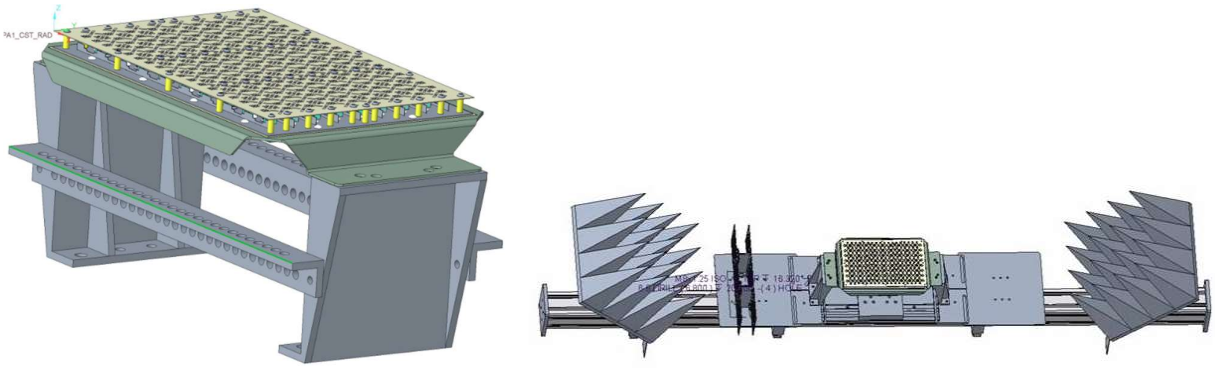

(a) Antenna fixation *(b) Antenna mounted on the rotation bar*

Figure 4.1. Antenna fixation supports made of non-metallic materials (a) to mount the antenna under test on the bar (b) of the rotation axis and swivel platform.

The following images illustrate the measurement setup.
Figure 4.1 (a) shows the antenna mounted on a custom plastic support structure. This setup is necessary to allow access to the rear antenna connectors for attaching the measurement cables.
Figure 4.1 (b) depicts the antenna, including the support structure, mounted on a rotatable mast used for azimuthal alignment.
Figure 4.2 (a) presents the antenna with removed array decoupling surface (ADS),
while Figure 4.2 (b) shows the antenna with the ADS installed, as it was configured during the measurements in the anechoic chamber.
Figure 4.3 provides an overview of the entire measurement chamber.

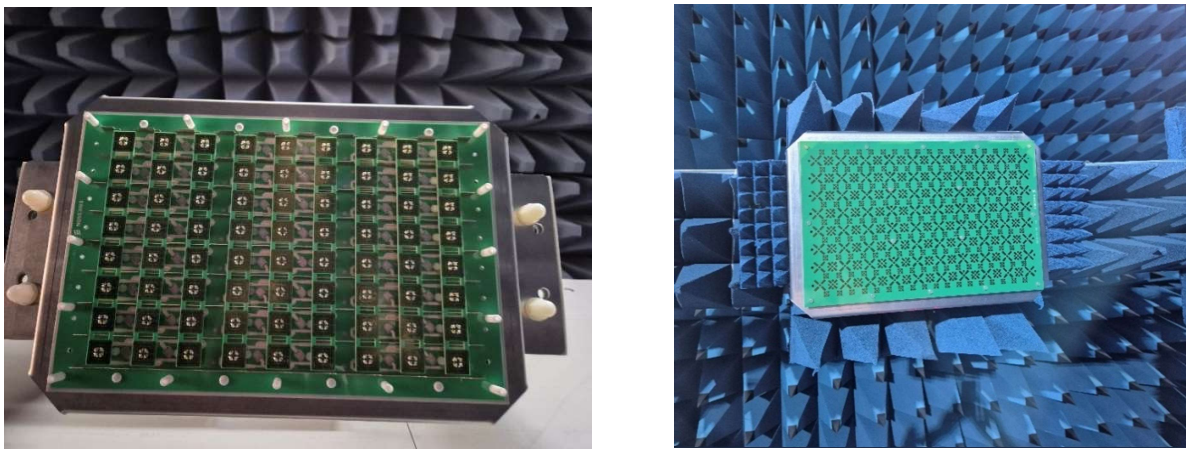

(a) Antenna with ADS *(b) Antenna without ADS*

Figure 4.2. Assembled antenna without ADS layer (a) and with a mounted ADS layer (b) and mounted in the chamber.

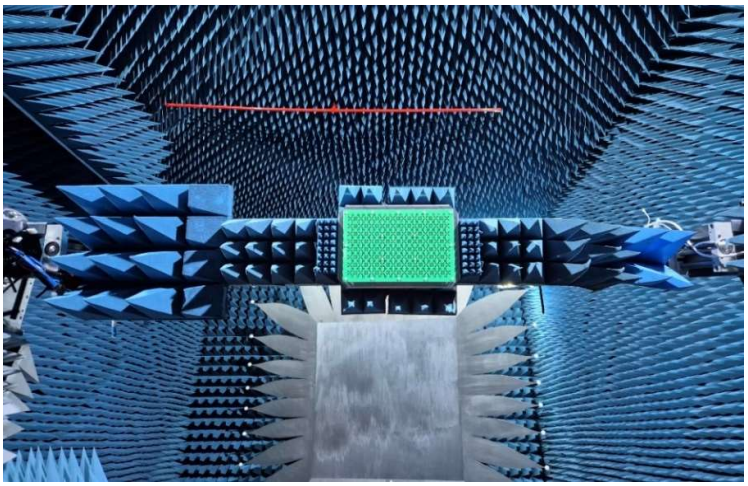

Figure 4.3. Antenna mounted in the compact test range measurement chamber, front perspective.

4.1.1 Antenna pattern on sub-sub-array level

This section presents the measurement results of the antenna's radiating pattern for a selected sub-sub-array. For this purpose, a sub-sub-array located at the center of the antenna was chosen. All unused antenna ports were terminated with 50-Ohm loads to prevent signal reflections.
As illustrated in Figure 4.4, a sub-sub-array consists of three dual polarized radiating elements,

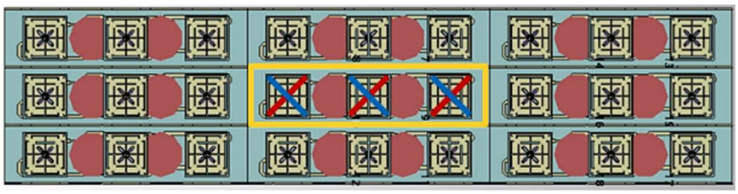

Figure 4.4.. Illustrates with the yellow box the sub-sub-array, in this representation, the antenna is positioned horizontally, with the antenna column extending from left to right.

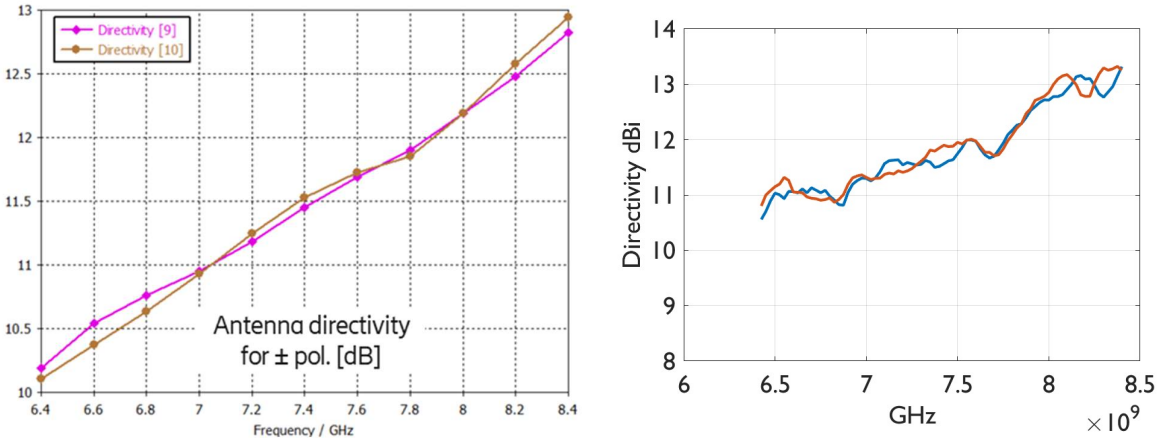

(a) EM simulation *(b) measurement result*

Figure 4.5.. Directivity on sub-sub-array level.

The antenna pattern directivity is calculated from the full sphere far field radiation pattern.
The full sphere far field radiation pattern consists of a co polarization component and a cross-polarization component. The directivity of an antenna increases at higher frequencies primarily due to the electrical size of the antenna; it becomes larger as frequency increases. Figure 4.6 compares the results of the electromagnetic (EM) simulation with the far-field measurement data for both antenna polarizations.
Directivity D is a measure of how concentrated the radiated power is in a particular direction. For aperture antennas (like patch arrays or parabolic dishes), directivity is approximately:

$$D \propto \left(\frac{A}{l^2}\right)$$

Where: λ is the wavelength of the signal, A is the aperture size (physical size of the antenna), since $l = \frac{c}{f}$ where f is frequency and c is the speed of light, we get:

$$D \propto f^2$$

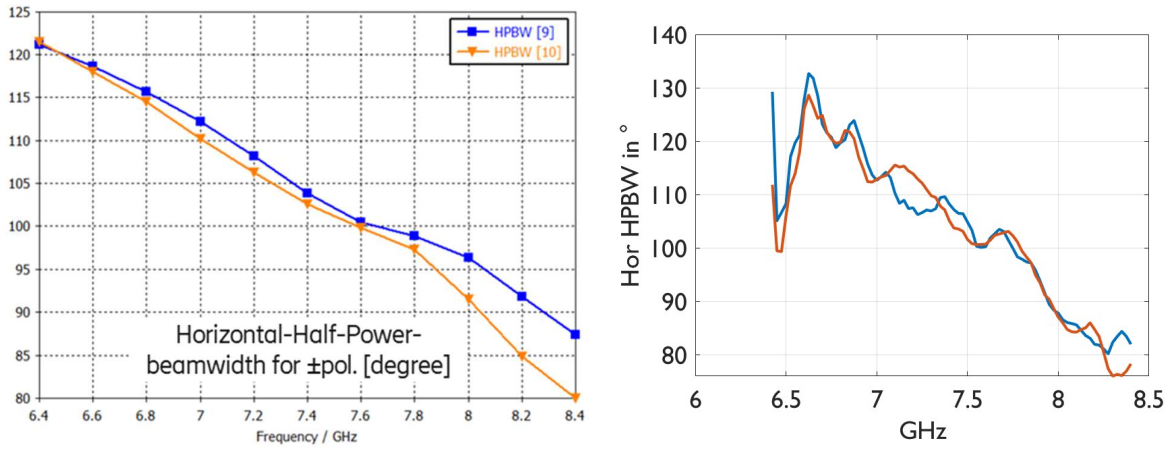

(a) EM simulation *(b) measurement result*

Figure 4.6. Horizontal -3dB half power beamwidth on sub-sub-array level.

The HPBW (half-power beamwidth) of an antenna is a measure of the angular width of the main lobe of the radiation pattern, defined as the angle between the two directions on either side of the main beam where the radiated power falls to half its maximum value (-3 dB points).
The HPBW becomes smaller at higher frequencies primarily due to the relationship between wavelength, aperture size, and beam width in antenna theory. The beam width of an antenna is approximately given by:

$$HPBW \propto \frac{l}{A}$$

With a constant antenna size A we get:

$$HPBW \propto \frac{1}{f}$$

So, as frequency increases, wavelength decreases, and the beam becomes narrower.

Side-lobes in phased array antennas are a natural result of wave interference from multiple elements. Their presence and strength depend on element spacing, phase and amplitude distribution, and the number of elements. The measurements in the vertical plane clearly demonstrate this behavior.

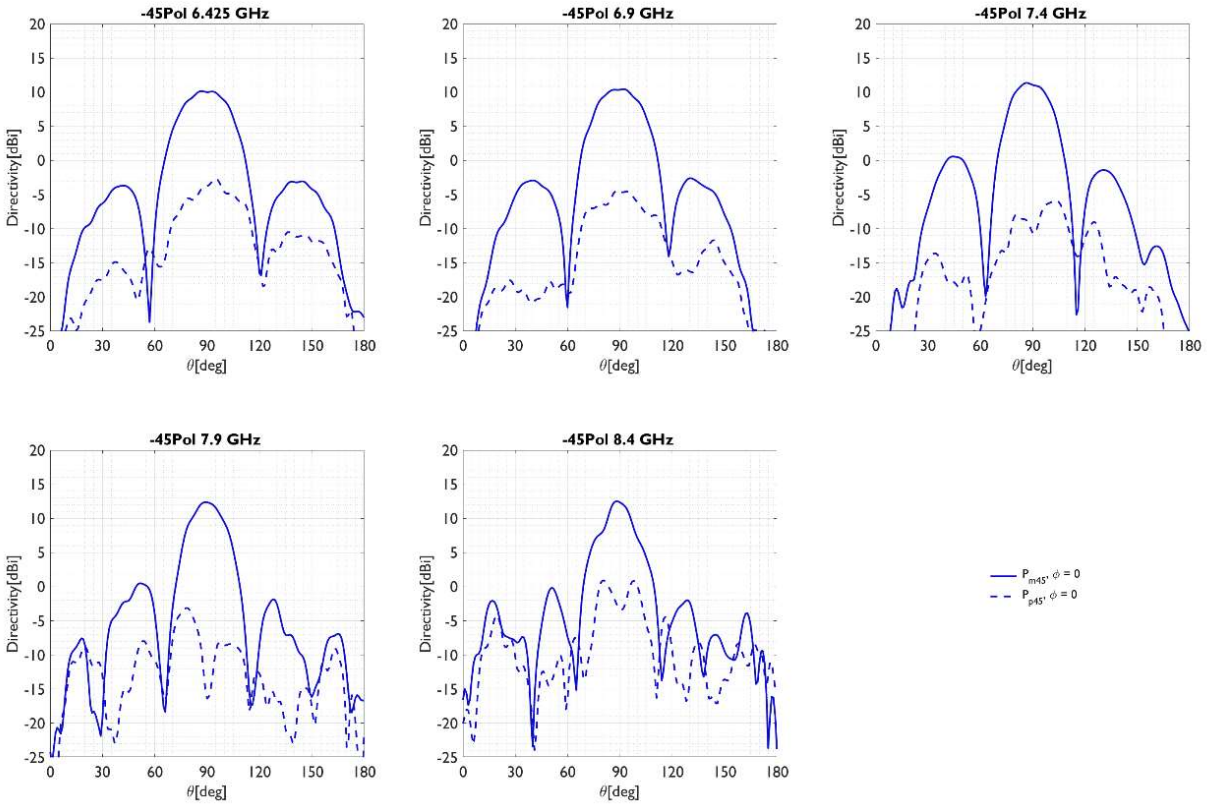

Figure 4.7. Vertical cut of the average beam pattern for the -45 deg polarization at different frequency points for the sub-sub-array.

• Horizontal average gain pattern:

Average gain pattern is defined as the linear average of the co-polar gain pattern per frequency and shall include all antenna unit ports. It can be calculated including all sub-array ports in the antenna unit or all sub-array ports with the same polarization in the antenna unit. All sub-array ports in the array shall be present and terminated with 50 Ω. The corresponding measurement curves for five frequency points are shown in Figure 4.8.

In a phased array antenna system, it is essential to ensure that the horizontal gain over the azimuthal angle Φ (phi) remains consistent across all operating frequencies. This requirement is critical for maintaining uniform performance in applications where the antenna must provide reliable coverage. For a series product, an average gain mask with Minimum and Maximum average gain at theta = 90 degrees (+tilt) is therefore defined. This was not constrained for this BS antenna implementation, but it is noticeable that the horizontal average directivity at 8.4 GHz is already quite wavy, Figure 4.8.

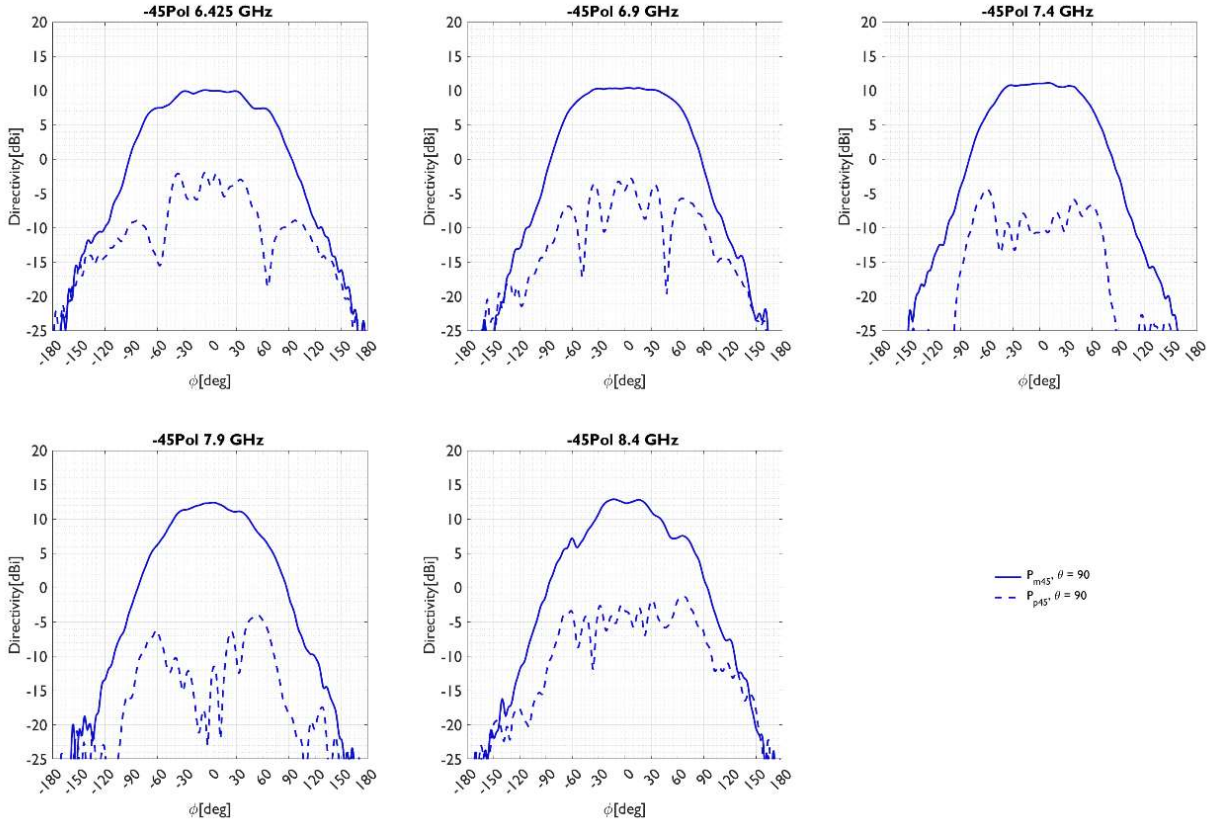

Figure 4.8. Horizontal cut of the average beam pattern for the -45 deg polarization at different frequency points for the sub-sub-array. Solid curve: co-polarization, dash curve: cross-polarization.

• Cross-polar discrimination:

The cross polar ratio is defined as the ratio between the co-polarization and the cross-polarization. It is specified over an angular area Φ (phi). In case of overlapping areas, the area with higher value takes precedence. The cross-polar Discrimination shall typically be more than 10 dB within the ±60 degree phi or >15 dB for ±30 degree phi from boresight. In Figure 4.8 the cross-polar discrimination is the delta of the Solid curve (co-polarization) and the dashed curve (cross-polarization).

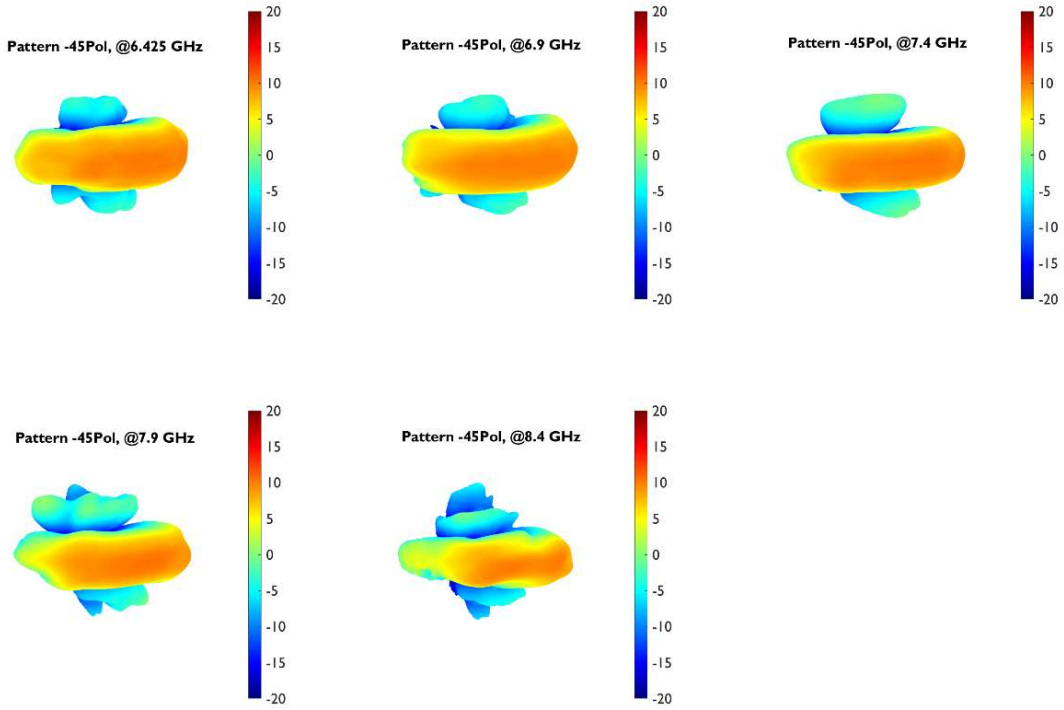

Figure 4.9. Three-dimensional presentation of the beam pattern on sub-sub-array level.

Figure 4.9: Each plot represents the radiation pattern of an antenna at a distinct frequency. The scale employs a color gradient to indicate varying intensity levels, with blue denoting lower intensity and red signifying higher intensity. The radiation patterns exhibit a generally symmetrical structure, characterized by a prominent central lobe and clearly visible upper and lower side lobes.

4.1.2 Antenna pattern zero-degree tilted antenna.

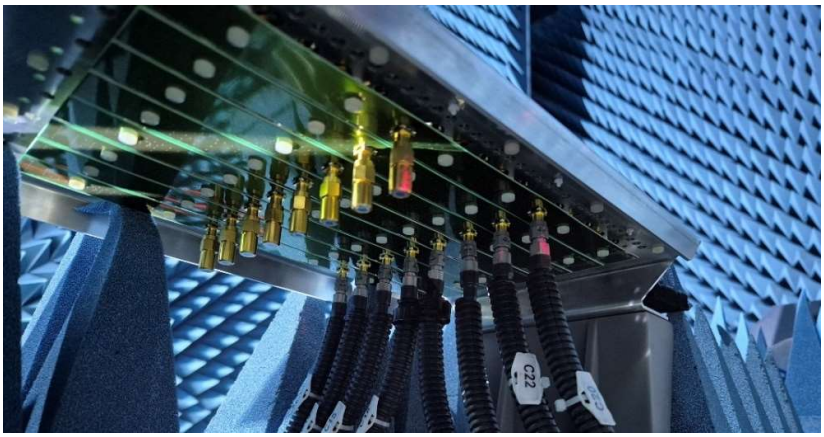

Figure 4.10. Antenna mounted in the measurement chamber. Eight antenna port can be measured in one run, all other port are terminated with 50 Ohm.

In the following measurements, a combination of three sub-sub-arrays—each corresponding to a single antenna column—was analyzed. In this configuration, the antenna theoretically exhibits a 4.77 dB higher directivity compared to an individual sub-sub-array level. The interpretation of the individual measurements follows the same principles outlined in Chapter 4.1.1 *Antenna pattern on sub-sub-array level* and will therefore not be repeated here.

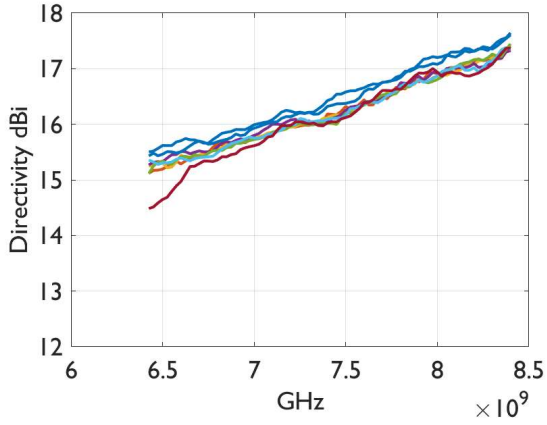

(a) Directivity

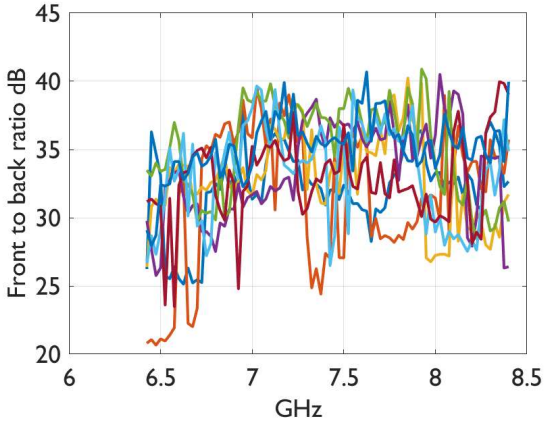

(b) Front to back ratio

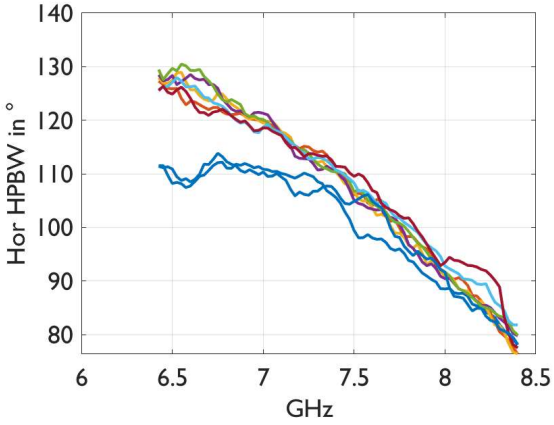

(a) Horizontal HPBW

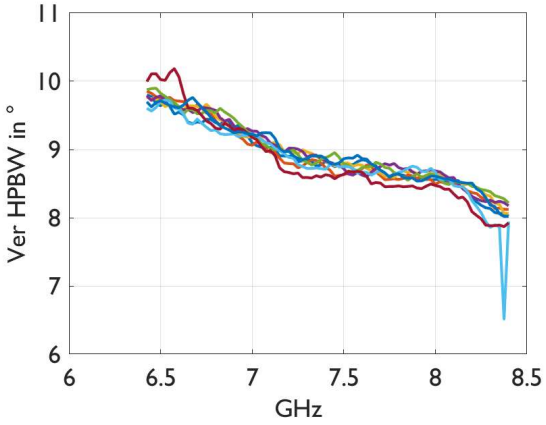

(d) Vertical HPBW

Figure 4.11. Results for the zero degree tilted antenna for one antenna polarization and all 8 antenna columns versus frequency. The graphs show the directivity, front to back ratio, horizontal -3dB half power beamwidth and vertical -3dB half power beamwidth.

The results of the far-field measurements demonstrate a threefold increase in directivity compared to the sub-sub-array level. This improvement is attributed to the tripled array length in the vertical direction and the significantly narrower beamwidth in the elevation plane.

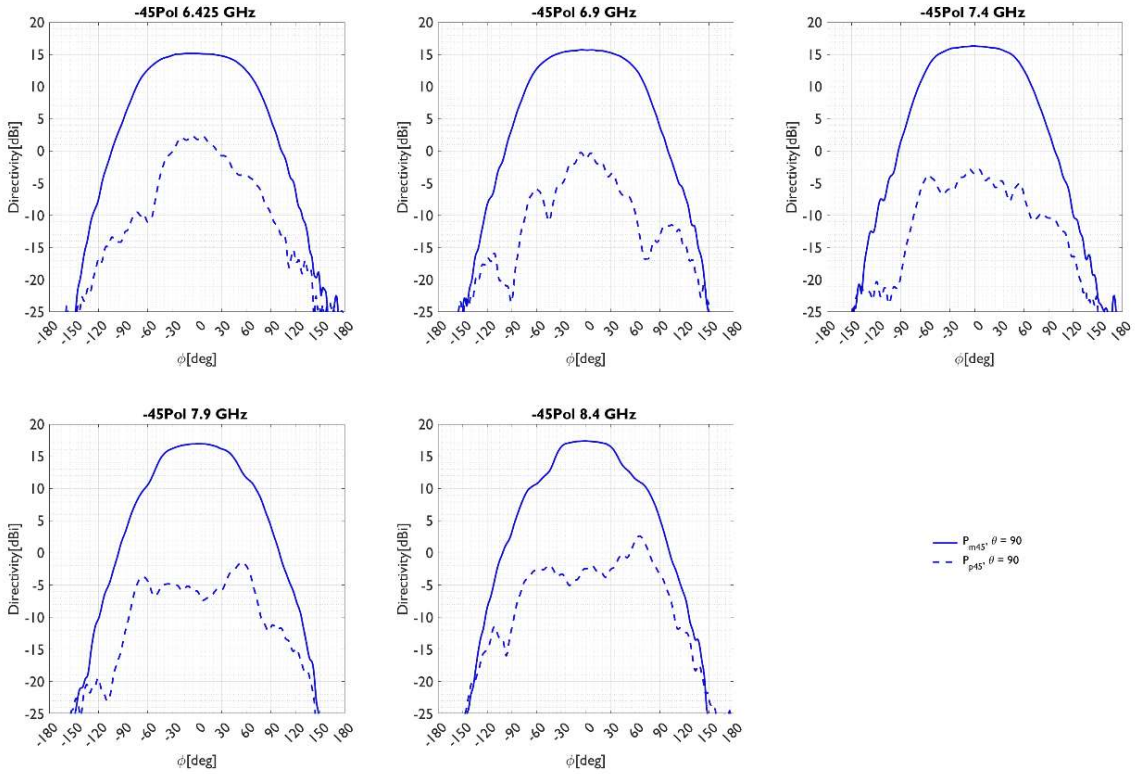

Figure 4.12. Horizontal cut of the average beam pattern for the -45 deg polarization at different frequency points for the zero degree tilted antenna. Solid curve: co-polarization, dash curve: cross-polarization.

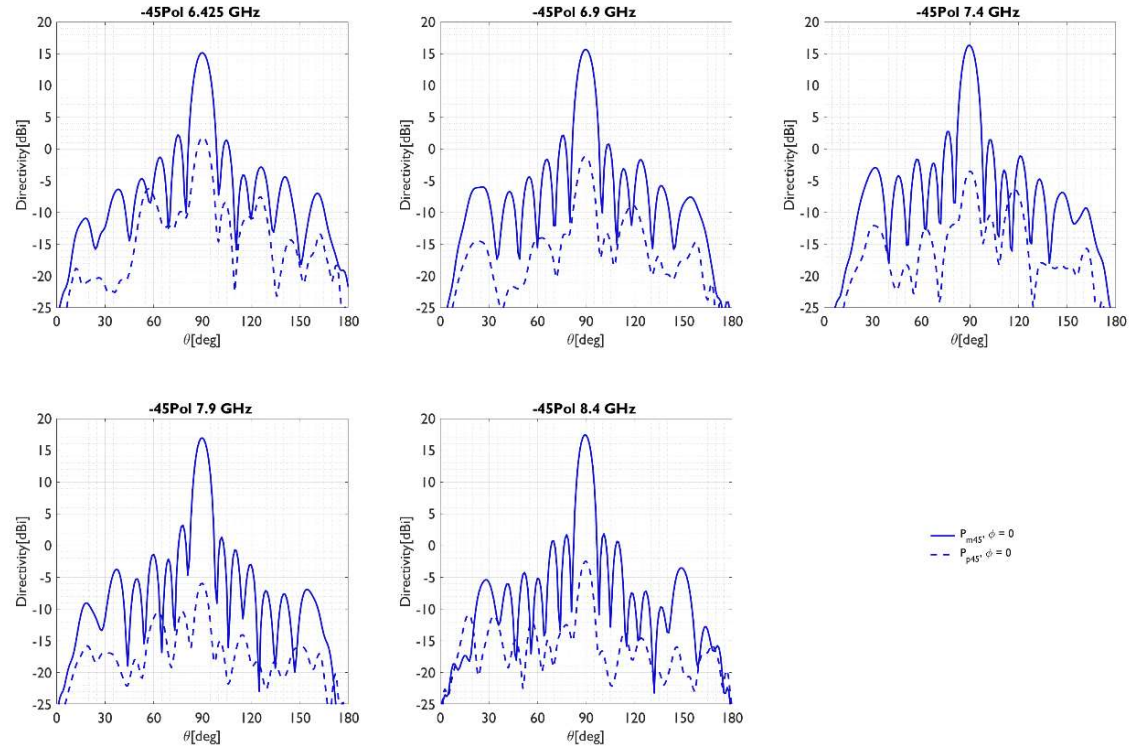

Figure 4.13. Vertical cut of the average beam pattern for the -45 deg polarization at different frequency points for the zero degree tilted antenna.

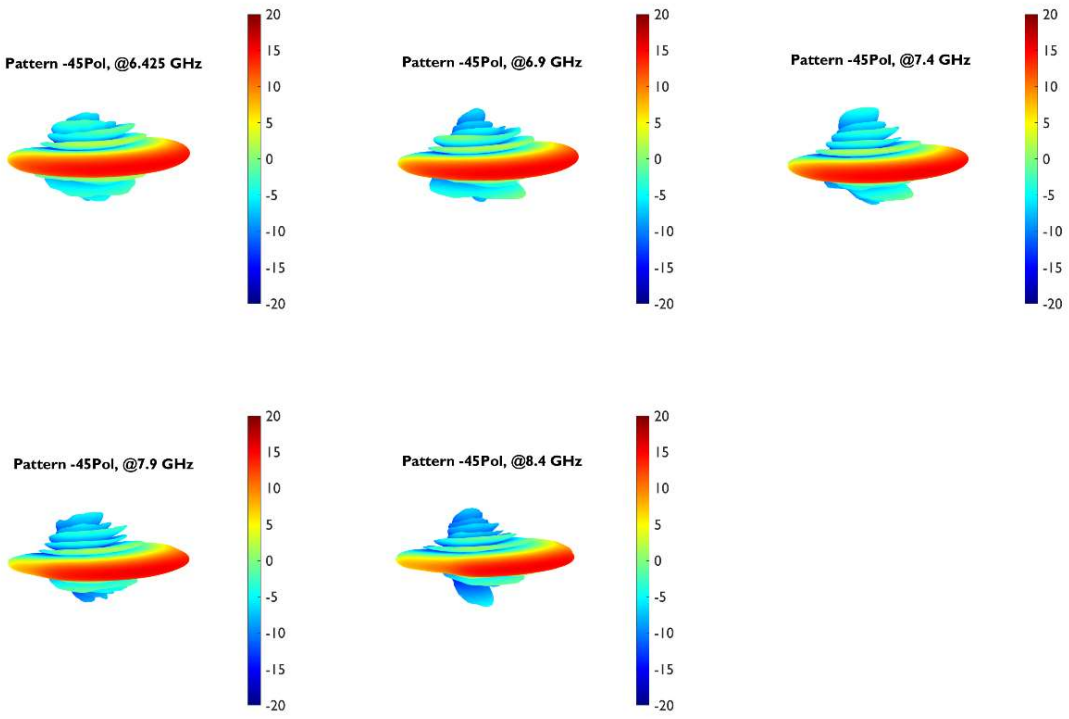

Figure 4.14. Three-dimensional presentation of the beam pattern of the zero degree tilted antenna.

When comparing the representation in Figure 4.14 with the three-dimensional beam pattern plot at the sub-sub-array level shown in Figure 4.9, a significantly narrower beam in the elevation direction can be observed. In contrast, the beam pattern in the azimuth direction remains unchanged.

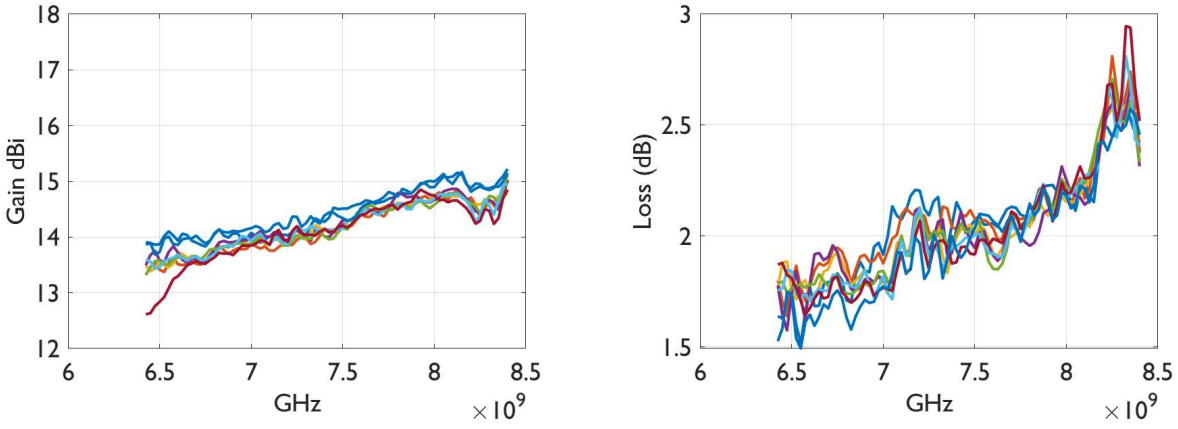

(a) Gain *(d) Losses*

Figure 4.15. Results for the zero degree tilted antenna, comparison of directivity and gain for one antenna column.

Antenna gain refers to the power accepted by the antenna; the gain does not include mismatch loss. The antenna gain is defined as total directivity minus losses. Figure 4.16 shows the measured result for

antenna gain and the calculated losses by subtracting the array directivity, Figure 4.11 (a) by the antenna gain. At mid-range frequencies, the losses are approximately 2 dB.

Following a rough estimation, this losses appears to be a plausible value. This encompasses the sum of all losses, consisting of:

- Return losses, losses due to not perfect matching of the TRX ports.
- SMA coaxial connector for the TRX ports.
- Micro-strip distribution network with approximately 180 mm in length on the back-plane and reflector board.
- Two times the miniSMP coaxial connectors on backplane and reflector board.
- MiniSMP bullet connection between back-plane network and reflector board.
- Losses in the radiator.
- ADS radome structure.

4.1.3 Antenna pattern 10-degree tilted antenna.

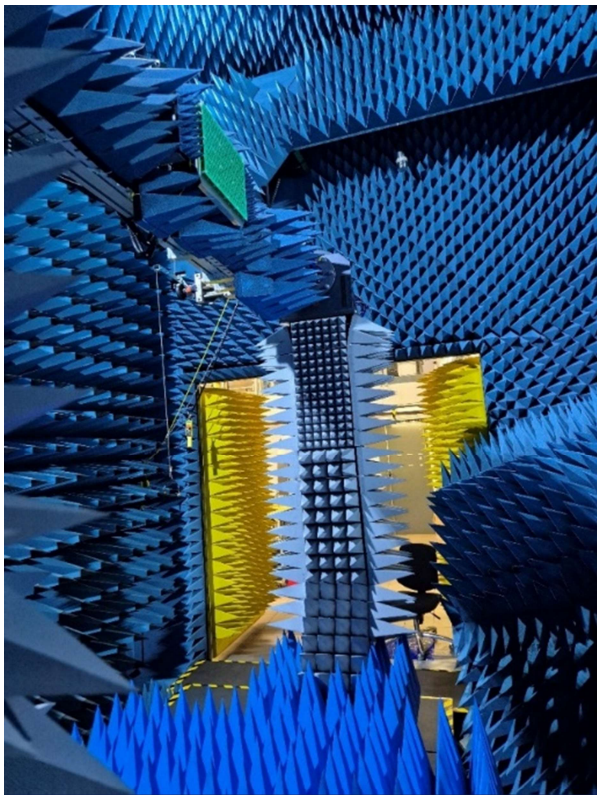

Figure 4.16. Antenna mounted in the far-field measurement chamber, side perspective.

This section presents the measurements of the antenna columns, as described in section 4.1.2 *Antenna pattern zero-degree tilted antenna*. The key difference here is that the rear backplane combining network incorporates a phase shifter. This phase shifter introduces a 10-degree tilt in the antenna array.

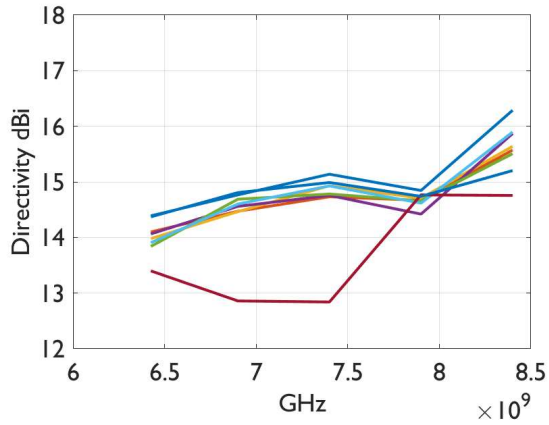

(a) Directivity

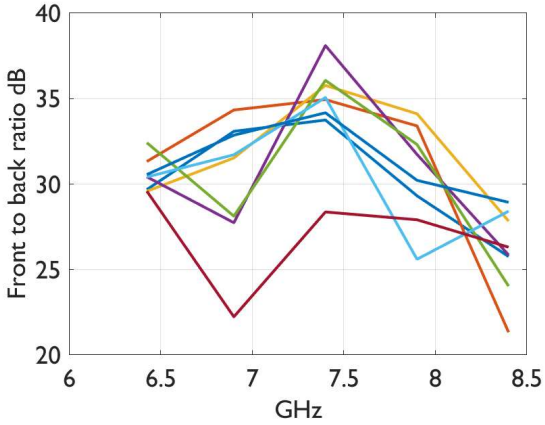

(b) Front to back ratio

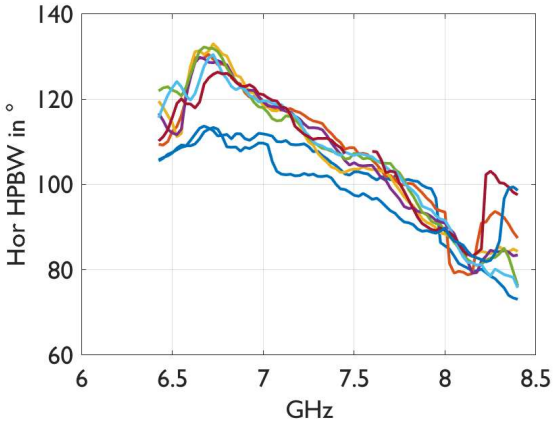

(a) Horizontal HPBW

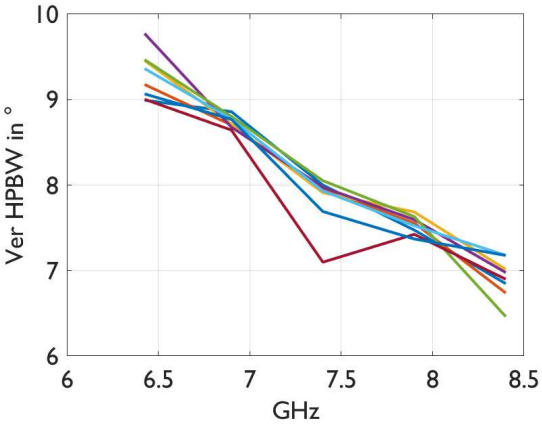

(d) Vertical HPBW

Figure 4.17. Results for the 10 degree tilted antenna for one antenna polarization and all eight antenna columns versus frequency. The graphs show the Gain, front to back ratio, horizontal -3 dB half power beam width and vertical -3 dB half power beam width.

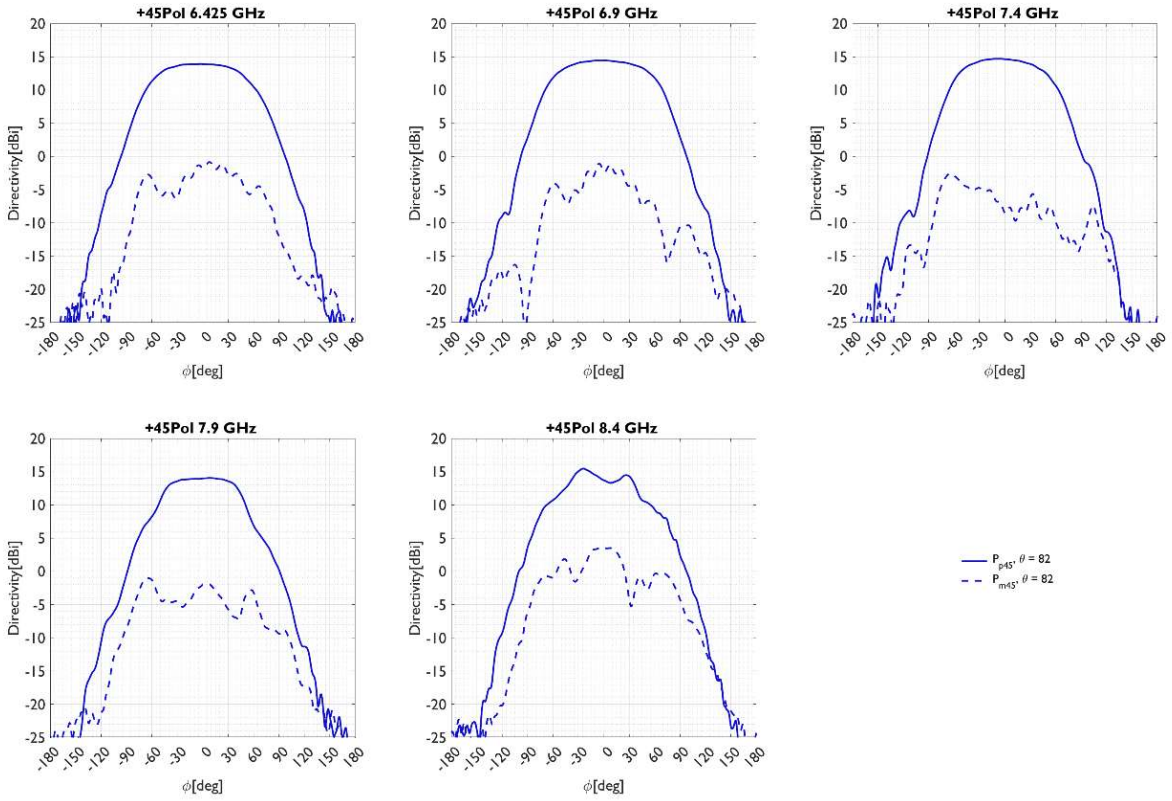

Figure 4.18. Horizontal cut of the average beam pattern for the +45 deg polarization at different frequency points for the 10 degree tilted antenna.

In the antenna unit equipped with the 10-degree tilt network, a significant deformation of the radiation pattern is observed, Figure 4.19 and Figure 4.20.

Notably, the side lobes reach levels nearly comparable to that of the main lobe. This effect arises from the fact that the vertical spacing between radiating elements in the array, set at 0.7 λ_c, is too large. As a result, implementing a 10-degree tilt is not considered optimal for this antenna dimensioning.

Nevertheless, it is valuable to examine this extreme case, as it provides insights into the limitations of the current array configuration. Based on the given array dimensions, a vertical beam tilt in the range of approximately +5° to −5° tilt angle is regarded as more practical and effective.

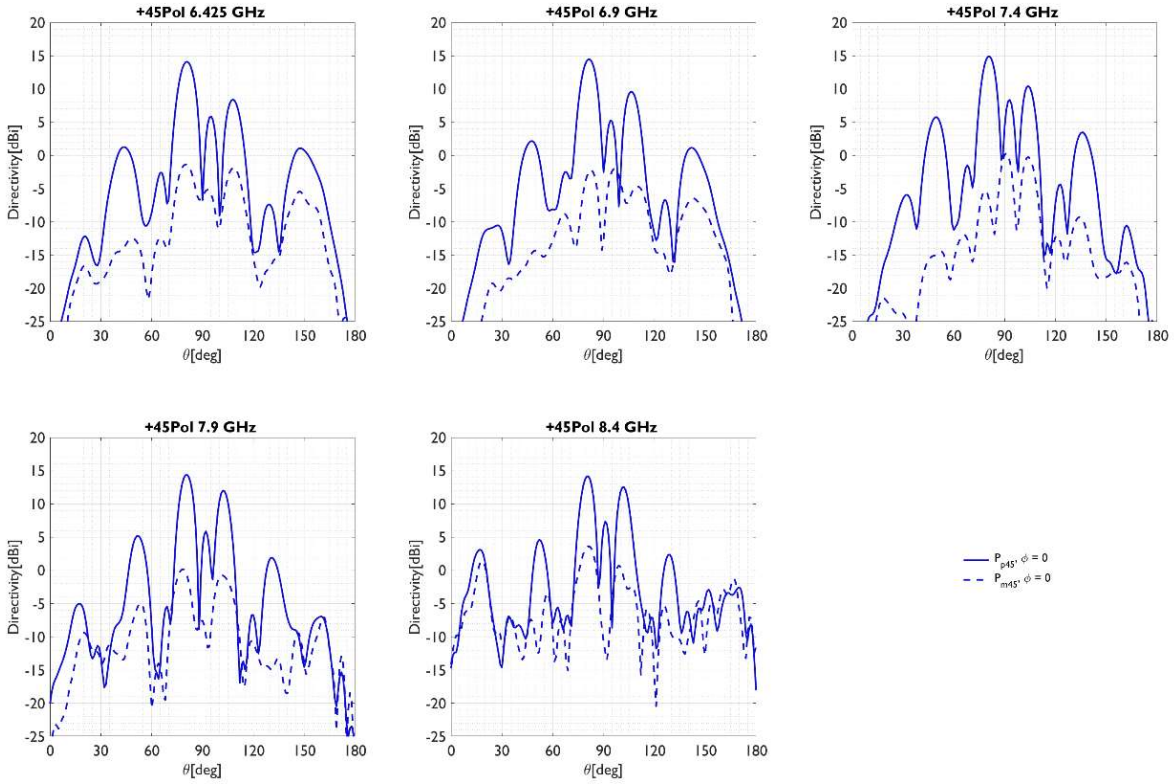

Figure 4.19. Vertical cut of the average beam pattern for the +45 deg polarization at different frequency points for the 10 degree tilted antenna.

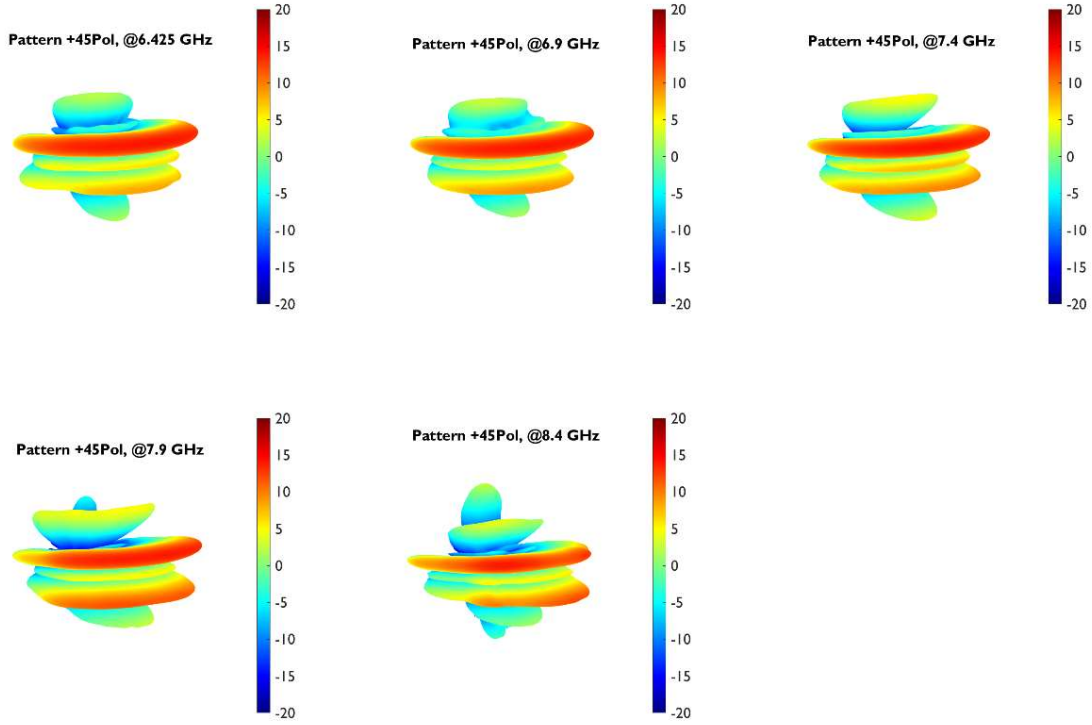

Figure 4.20. Three-dimensional presentation of the beam pattern of the 10 degree tilted antenna.

5 Conclusion

The measurement results for an ATG antenna for the 7 GHz band were presented in this document. The ground BS antenna consists of PCB-based radiators with an ADS to mitigate radiator coupling.
This work has demonstrated the potential of a novel antenna technology featuring wide-band radiating elements, which shows strong promise for future industrial applications. The measurement results of scattering parameters and radiation patterns exhibit a high degree of consistency with simulation data, confirming the validity of the design approach and the accuracy of the modeling techniques used.
The successful construction and testing of two hardware prototypes enabled not only the validation of the antenna's electrical performance but also provided valuable practical insights into the manufacturing process. In particular, the assembly procedures-such as soldering and mechanical integration—revealed important considerations for transitioning from prototype development to scalable production.
Overall, the results confirm that the proposed antenna concept is both technically sound and manufacturable, laying a solid foundation for further optimization and industrial implementation.

6 Bibliography

[1] L. N. Ribeiro, S. Hastürkoglu, M. Jacob, P. Gentner, J. Graevendieck and T. Mann, "Simulation Framework for Investigation of Antennas Integrated in Flying Vehicles and Their Performance in Real-World 3D Network Scenarios," CELTIC-Next Project 6G-Sky D2.2.1, 2023.

[2] CELTIC-Next Project 6G-Sky, "Memorandum 2.2 Antenna Performance," 2025.

[3] CELTIC-Next Project 6G-Sky, "Deliverable D2.2.3 Ground Base Station Antenna Requirements," 2024.

[4] K.-L. Wu, C. Wei, X. Mei and Z.-Y. Zhang, "Array-antenna decoupling surface," *IEEE Transactions on Antennas and Propagation,* vol. 65, p. 6728–6738, 2017.